Article

Distribution of Weakly Interacting Atoms and Molecules in Low-Temperature Amorphous Solid Water

Michelle Sykes Akerman, Roey Sagi, Hiley Iny, and Micha Asscher*

Cite This: *J. Phys. Chem. A* 2022, 126, 8037−8048

Read Online

ACCESS | 　 Metrics & More | 　 Article Recommendations

ABSTRACT: Understanding the distribution and mixing of atoms and molecules in amorphous solid water (ASW) at low temperatures is relevant to the exploration of the astrochemical environment in the interstellar medium (ISM) that leads to the formation of new complex molecules. In this study, a combination of temperature programmed desorption (ΔP-TPD) experiments and Ne^+ ion sputtering is used to determine the extent of mixing and distribution of guest atoms and molecules within thin ASW films deposited at 35 K on a Ru(0001) substrate, prior to sputtering. The mixing of krypton atoms and methyl chloride molecules within thin ASW films is directed by the physical properties of the respective species and the nature of their interaction with the host water molecules. While the $Kr-H_2O$ interaction may be described as a weak van der Waals attraction, the CD_3Cl-H_2O interaction can be characterized as weakly hydrophobic in nature. This leads to differences in the level of homogeneity in mixing and distribution of the guest species in the ASW film. Both krypton atoms and methyl chloride molecules reveal a propensity to migrate toward the ASW−vacuum interface. The krypton atoms migrate through both diffusion and displacement by incoming H_2O molecules, while the methyl chloride molecules tend to move toward the vacuum interface primarily via displacement. This behavior results in more homogeneous mixing of Kr in ASW at 35 K compared to the dipole moment containing molecule CD_3Cl. As a general outcome of our study, it is observed that mixing in ASW at low temperatures is more homogeneous when the guest atom/molecule is inert and does not possess a constant dipole moment.
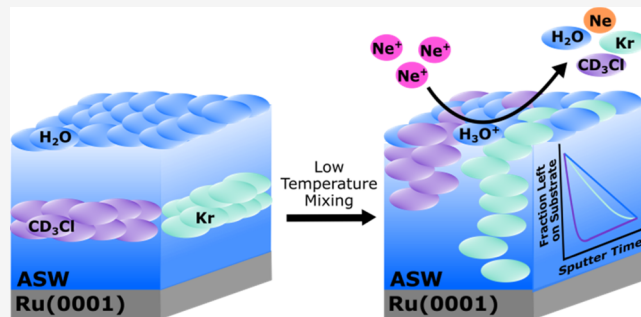
1. INTRODUCTION

The physics and chemistry of amorphous solid water (ASW) is of interest because of its abundance in our universe. Water-dominated ices (in the form of ASW) are adsorbed on low-temperature dust grains in the interstellar medium (ISM). The icy mantles may also contain small molecules such as CH_3OH, CO, CO_2, NH_3, CH_4,[1,2] and even CH_3Cl,[3,4] in varying (smaller) abundances with respect to water. Ice-coated dust particles in the ISM are subject to bombardment by energetic ions, electrons, and UV photons that can induce chemical reactions between guest molecules adsorbed inside ASW films that grow on the dust grain surfaces. Since the proximity of molecules in the ASW is critical to the formation of new and more complex molecular products upon exposure to energetic irradiation, the distribution of the guest molecules within the host ASW film influences the types of molecules that can be formed. Additionally, this information enables the laboratory preparation of model ASW-dominant films that are of astrochemical relevance (in terms of guest molecule distribution) for further study. Moreover, the behavior of guest atoms and molecules in porous ASW films can be used as a model for understanding fundamental low-temperature interactions between porous solids and caged atoms/molecules.

Here, a study of the structure and internal distribution of thin ASW films containing krypton (Kr) atoms or the polar molecule methyl chloride (CD_3Cl), both of which interact relatively weakly with water molecules, is presented. There are several studies of krypton and methyl chloride in ASW ices. Studies involving krypton and ASW use krypton as a probe for exploring the morphological changes that take place in the amorphous water ice upon heating.[5−8] A model for the diffusion of inert gases through molecular solid films near their glass transition temperatures assumes that the inert atoms are homogeneously distributed throughout the films, regardless of their initial position.[9] Experimental studies confirm this model, but only for films thicker than 50 ML.[10] Thinner films display enhanced diffusivity and deviate from the above models. These studies all utilize temperature programmed desorption (TPD)
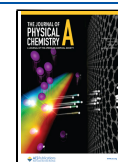
experiments that require heating of the films. An understanding of the diffusion and dispersion of krypton atoms in ASW at low temperatures that are typical to the ISM is lacking.

Thin films of several layers of methyl chloride and water have been studied to understand the interaction between the two molecules on metal surfaces.[11,12] H_2O and CH_3Cl have similar gas phase dipole moments of 1.85 and 1.87 D, respectively. In contrast to H_2O molecules, which display attractive forces toward one another via hydrogen bonding, CH_3Cl molecules repel one another when adsorbed on a metal substrate at sub-monolayer densities and do not display attractive forces toward H_2O.[11,12] Additionally, previous studies show that adsorbed methyl chloride molecules are compressed and caged as a result of water molecules that subsequently accumulate on the substrate and form a film. The methyl chloride guest molecules are released from the ASW film upon heating and crystallization of the water ice in a "molecular volcano" process.[11] The diffusion of other chloro-methanes through ASW has been explored.[13,14] One study shows that CCl_4 cannot diffuse through ASW at temperatures of 110–150 K, while $CHCl_3$[13] and CH_2Cl_2[14] do diffuse through ASW in this temperature range. The lack of diffusivity of CCl_4 in ASW is attributed to its inability to penetrate the hydrogen-bonded network in the ice film. The diffusivity of CH_3Cl in ASW has not yet been investigated, although the results described in ref 14 suggest that CH_3Cl will be able to diffuse at temperatures > 110 K.

While some aspects of the behavior of krypton and methyl chloride in ASW have been explored, there are no reports of the distribution or dispersion of these atoms/molecules in thin ASW films grown at low temperatures, where the film's porosity is considered to be high. In this study, the mixing and distribution of Kr atoms and CD_3Cl molecules in a thin (26 ML) ASW film grown at 35 K are studied. It is well documented that the morphology and porosity of ASW films is affected by the growth temperature of the films.[6,15−20] In this study, the films were all grown at one temperature, removing the effect of pore size on the mixing from this study. The low temperature of 35 K was chosen to make this study relevant to processes that may be occurring in the ISM. Ne^+ ion sputtering and temperature programmed desorption (ΔP-TPD) experiments are used to determine the extent of mixing and the distribution of Kr atoms and CD_3Cl molecules within the low-temperature ASW films. The Ne^+ sputtering was employed to gradually remove layers of the prepared Kr@ASW and CD_3Cl@ASW films. Post-sputtering ΔP-TPD experiments measure the amount of guest and host molecules remaining on the substrate, giving an indication of how the guest molecules are distributed within the ASW films at 35 K prior to the sputtering process.

2. EXPERIMENTAL SECTION

Films of ASW containing Kr atoms or CD_3Cl molecules were grown on a Ru(0001) single-crystal substrate held in the center of an ultrahigh vacuum chamber with a base pressure of 2×10^{-10} Torr. The top and bottom edges of the 8 mm × 8 mm, 2 mm thick Ru(0001) substrate were spot-welded to 0.4 mm tantalum wires, attaching the substrate to a $x−y−z$ manipulator on a rotatable stage (McAllister). This is obtained via two tantalum legs 3 mm thick connected to two copper rods and a sapphire disc attached to the bottom of a closed cycle He cryostat (Lakeshore/Janis) to cool the sample down to a minimum temperature of 30 K. The sample temperature was

stabilized between 30 and 300 K using a Lakeshore 335 controller, employing a silicon diode sensor to monitor the temperature at the sample holder. In addition, a K-type thermocouple (chromel−alumel) was spot-welded to one side of the ruthenium substrate to measure the sample temperature with an accuracy of ±1 K. A LabView algorithm enabled controlled heating and cooling of the sample temperature in the range of 30−1450 K. The Ru(0001) is cleaned daily by a 15 min sputtering employing 1000 eV Ne^+ ions and subsequent annealing at 1450 K for 10 min. Films of H_2O, Kr, and CD_3Cl were deposited on the substrate through backfilling the vacuum chamber (ensuring identical coverage all over the sample and all other cooled surfaces) with the designated gaseous species until the desired film thickness was obtained in units of Langmuir (1 L = 10^{-6} Torr s). Units of monolayer (ML) are determined for each adsorbed species by identifying the onset of multilayer desorption for each molecule/atom using exposure-dependent temperature pro-grammed desorption (ΔP-TPD) experiments (assuming unity sticking probability at 35 K). ΔP-TPD experiments are conducted using a quadrupole mass spectrometer (QMS), (RGA 200, SRS) to detect the masses of species desorbing as the substrate temperature is ramped at a fixed rate, typically 1 K/s. To study the low-temperature distribution and mixing of Kr atoms or CD_3Cl molecules within ASW, an ion sputtering gun (Varian) is used to bombard ASW films containing Kr atoms or CD_3Cl molecules at 35 K employing a Ne^+ ion beam at an energy of 800 eV that uniformly covers the entire substrate area. The Ne^+ sputtering gradually removes layers of the prepared films. ASW films 26 ML thick are completely removed from the substrate following 16 min of sputtering at this beam energy at a typical substrate to ground current of 2.6 μA. After the designated sputtering time (0−16 min), a ΔP-TPD experiment is conducted to determine the amount of material left on the substrate, by simultaneously detecting both the guest (Kr or CD_3Cl) and host (H_2O) species. This procedure ensures that the removal of guest−host films occurs following the mixing process. As will be discussed below, the Ne^+ ion collisions may influence the top 2−3 ML of the film, but do not affect the distribution or mixing event itself, which is completed prior to the sputtering process.

3. RESULTS AND DISCUSSION

The following work explores whether there is a systematic, physical concept that directs different atoms and molecules in their low-temperature distribution and mixing in ASW. A probe molecule and an atom that interact weakly with the ASW matrix were used to investigate how the guest molecule's (or atom's) physical properties affect its low-temperature propensity to mix and migrate within thin ASW films (≤50 ML thick).

ASW film thickness of 26 ML was chosen since this thickness allows for the simultaneous detection of H_2O (m/z = 17), and the guest atom or molecule (Kr (m/z = 84) and CD_3Cl (m/z = 53)) by the QMS in a single ΔP-TPD scan, avoiding signal saturation problems. The effect of a strong electric field on the guest molecule distribution can be ignored since the Ne^+ ion sputtering experiments conducted at 800 eV do not lead to stable charging of thin ASW films, as detected by our in situ Kelvin probe. Stable positive charging only occurs on significantly thicker layers of ASW.[21]

3.1. Krypton Atom Mixing and Distribution in ASW at 35 K. Kr atoms are expected to interact weakly with the host
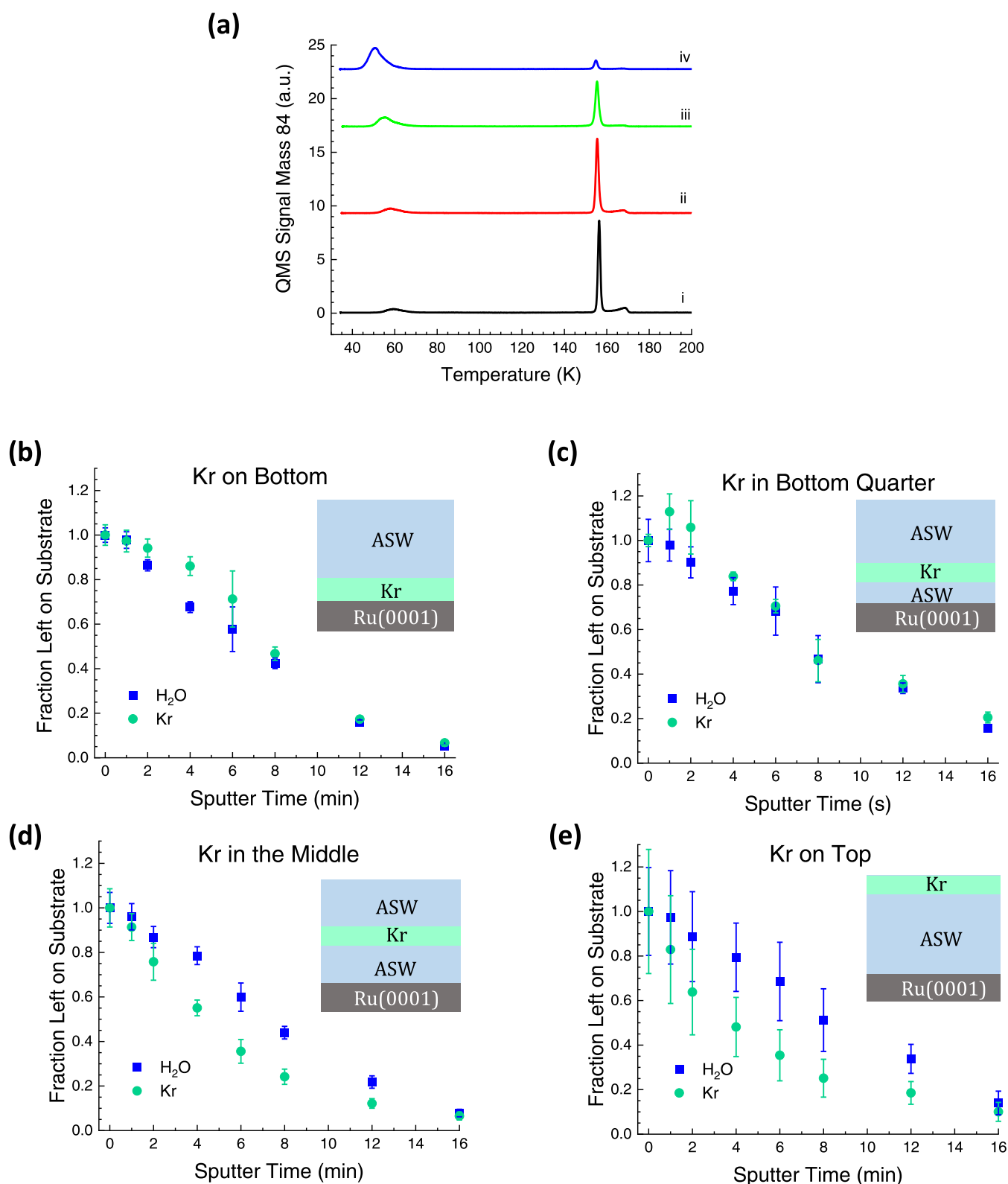
Figure 1. 2 ML Kr at different initial locations in 26 ML ASW adsorbed at 35 K followed by (a) temperature programmed desorption measurements (ΔP-TPD) of Kr (atomic mass to charge ratio, $m/z = 84$) at a heating rate of 1 K/s. (i) 2 ML Kr initially in direct contact with the ruthenium substrate, subsequently covered by 26 ML ASW (black), (ii) 2 ML Kr in the bottom quarter of 26 ML ASW (red), (iii) 2 ML Kr in the middle of 26 ML ASW (green), and (iv) 2 ML Kr on top of 26 ML ASW (blue). (b−e) Sputtering of 2 ML Kr in 26 ML ASW@35 K with 800 eV Ne⁺ ions (~2.6 μA) for 0−16 min. The normalized fractions (area under all of the corresponding ΔP-TPD peaks) of Kr ($m/z = 84$, green circles) and H_2O ($m/z = 17$, blue squares) remaining on the substrate are plotted versus sputtering time. The indicated error is due to the average of at least two measurements. The initial position of the 2 ML Kr is indicated in the inset schemes: (b) bottom (directly on the substrate), (c) bottom quarter, (d) middle, and (e) top.

water molecules due to their inert character. When 2 ML of Kr is initially adsorbed at different locations within 26 ML of ASW (as a sandwich) on a Ru(0001) substrate at 35 K, differences in the ΔP-TPD profiles of Kr ($m/z = 84$) are observed (Figure 1a). The three ΔP-TPD peaks correspond to different types of Kr-atom desorption, depending on the location of the atoms within the ASW and their interaction with their surroundings. Kr atoms that are located on or near the top surface of the ASW film are surrounded mostly by other Kr atoms and can diffuse through ASW pores. These atoms desorb at low temperatures[22] between 50 and 60 K ("diffusion" peak). This temperature is higher than Kr multilayer desorption from clean ruthenium, which occurs at 43 K,[23] indicating that the Kr atoms are in direct contact with a few water molecules that stabilize them. The remaining Kr atoms (majority) are released to the vacuum in an "atomic volcano" peak as a result of the ASW crystallization at 156 K or are "trapped" until they desorb together with the multilayer of water at 167 K.[24,25] Figure 1a shows that as the initial Kr atoms' location approaches the ASW−vacuum interface, the low-temperature diffusion peak grows in intensity and shifts to lower temperature, while the atomic volcano and trapped peaks decrease in intensity but are observed at the same temperature. This suggests that the initial Kr location dictates where the majority of the Kr atoms reside within the ASW film and the nature of their chemical environment prior to any heating.

Kr@ASW films varying in initial Kr-atom location are sputtered by 800 eV Ne$^+$ (∼2.6 μA ion current measured between the ruthenium substrate and ground) for 0−16 min at 35 K to slowly remove layers of the film. After each designated sputtering time, a ΔP-TPD measurement is taken to determine how much Kr and H$_2$O remain on the Ru(0001) substrate after sputtering. The normalized fraction of Kr and H$_2$O remaining on the surface is plotted versus the sputtering time (Figure 1b−e). In this way, the distribution of the Kr atoms within the ASW film is investigated.

When the Kr@ASW films are bombarded by 800 eV Ne$^+$ ions at 35 K, some of the Kr atoms become further embedded in the surrounding top layers of the ASW matrix, rather than being sputtered away to the vacuum. This is evident from the ΔP-TPD profiles that show a reduction in the intensity of the low-temperature diffusion peak and an increase in the intensity of the atomic volcano and trapped peaks upon sputtering for only 1 min (Figure 2). The changes in the ΔP-TPD profiles suggest that the sputtering causes a change in the Kr atoms' chemical environment by increasing their extent of entrapment within the surrounding water molecules (each Kr atom has more H$_2$O neighbors). This phenomenon is seen most dramatically when the Kr atoms are placed on top of ASW and the film is sputtered for only 1 min. For a nonsputtered Kr@ASW film where Kr atoms are placed on top of the ASW, the percentage of the Kr atoms desorbing in the diffusion, atomic volcano, and trapped peaks are 87.6, 10, and 2.4% respectively. After 1 min of sputtering, 20% of the Kr atoms are removed, 3.6% desorb in the diffusion peak, 70% desorb in the atomic volcano peak, and 5.4% desorb in the trapped peak. One minute of sputtering already causes a change in the chemical environment of the Kr atoms within the ASW matrix, but not necessarily their location (in terms of depth) in the film. Even when Kr atoms are initially placed directly on the ruthenium substrate, the chemical environment of the Kr atoms is influenced by sputtering. After 1 min of sputtering, only 3% of the Kr atoms are removed from the film, but the
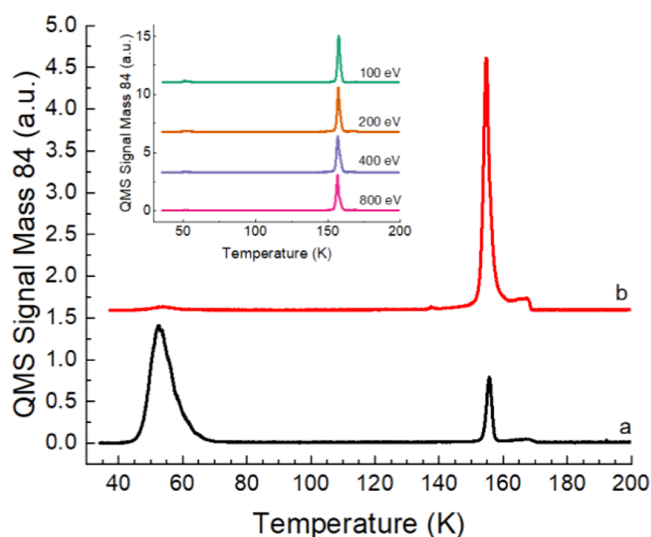
Figure 2. ΔP-TPD of 2 ML Kr ($m/z = 84$) on top of 26 ML ASW: (a) no sputtering and (b) after 1 min of sputtering with 800 eV Ne$^+$ at 35 K. Inset: The effect of Ne$^+$ kinetic energy on Kr ΔP-TPD.

percentage of atoms desorbing in the diffusion peak decreases from 20 to 0.7%, while the percentage of atoms desorbing in the atomic volcano and trapped peaks increases from 66.5 to 79.2% and from 13.5 to 17.1%, respectively. While the sputtering process causes the Kr atoms to become more deeply embedded in the film and surrounded by H$_2$O molecules, the atoms probably do not migrate far from their initial location (depth-wise) in the ASW. At an energy of 800 eV, the Ne$^+$ ions are not likely to knock the Kr atoms further than 2 ML deep into the ASW film. This is because of the relatively large mass of the Kr atoms compared with that of the collider in addition to the effective dissipation of Ne$^+$ kinetic energy within the ASW film. The Ne$^+$ ion beam energy was reduced to 100 eV to examine the possible effect of the Ne$^+$ kinetic energy on the Kr distribution in the ASW film (inset of Figure 2). We found that even when the Ne$^+$ beam energy is reduced, similar distributions of the atoms are obtained. Lower Ne$^+$ beam energies mainly reduce the removal rate of the atoms and molecules in the film. It is likely that bombardment by Ne$^+$ ions induces a local restructuring, primarily near the location of impact at the top ASW layers.

To better understand the effect of sputtering on the Kr distribution, we performed experiments that are summarized in Figure 3. In these experiments, 1 ML of Kr atoms (used as sensors) are adsorbed on top of ASW films 26 ML thick. The difference between the experiments is only the growth temperature (T_{gr}) of the ASW films. In addition, these ΔP-TPD spectra for Kr ($m/z = 84$) are compared with a film that was annealed to 150 K for 5 min (to become hexagonal crystalline ice—I$_h$)[26,27] and a sputtered film that was prepared at 35 K. The ΔP-TPD profile for Kr adsorbed on the nonsputtered film grown at 35 K displays three peaks for Kr— a diffusion peak at 52 K, an atomic volcano peak, and a trapped peak. In contrast, the ΔP-TPD profile for Kr adsorbed on the presputtered ASW grown at 35 K displays only a diffusion peak at 42 K and a trapped peak. ΔP-TPD profiles of 1 ML of Kr on ASW films grown at temperatures ranging from 35 to 70 K and on a crystalline film ($T_{gr} = 35$ K, annealed to 150 K and cooled to 35 K before the 1 ML Kr adsorption) reveal that Kr atoms can only penetrate ASW pores (as reflected by the atomic

(a)

(b)
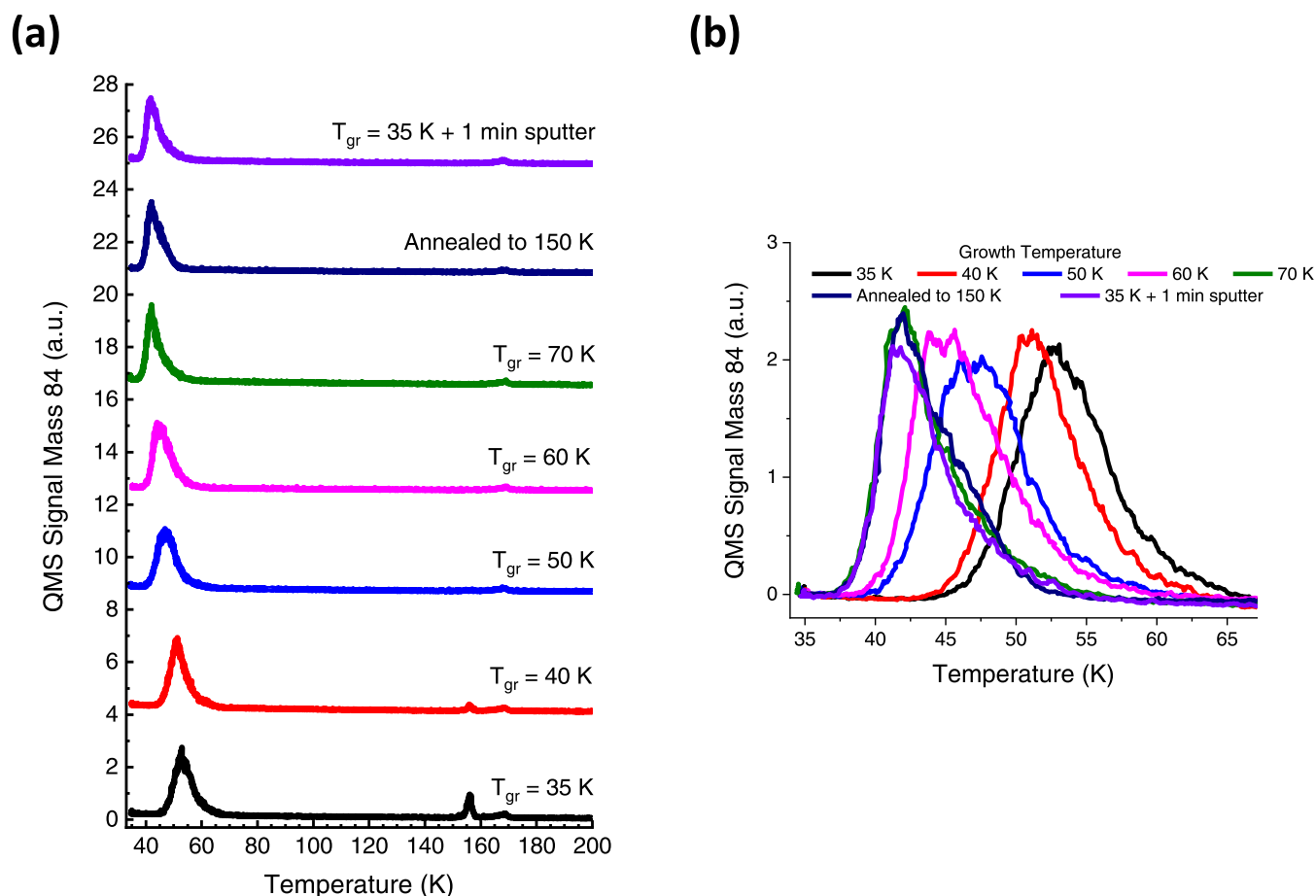
Figure 3. (a) ΔP-TPD profile of 1 ML of Kr ($m/z = 84$) adsorbed on top of 26 ML of ASW grown at 35 K (black profile) is compared to ΔP-TPD profiles of 1 ML of Kr adsorbed on top of ASW films grown at 40 K (red profile), 50 K, (blue profile), 60 K (magenta profile), and 70 K (green profile), 1 ML of Kr adsorbed on top of a 26 ML thick crystalline film obtained by annealing the ASW film at 150 K for 5 min (navy profile) and 1 ML of Kr adsorbed on top of 26 ML of ASW grown at 35 K that was sputtered by 800 eV Ne+ ions for 1 min (purple profile). The profiles are offset for clarity. (b) Enlargement and overlay of the profiles shown in panel (a) to see how the low-temperature peak shifts to lower temperatures with increasing growth temperature and sputtering after growth at 35 K.

volcano desorption) when the films are grown at temperatures below 70 K. At these low temperatures, the relatively broad Kr-atom desorption peak shifts to higher temperatures (from 42 K@70 to 52 K@35 K) and an atomic volcano peak is evident only for growth temperatures below 45 K. The shift of the desorption peak to higher temperatures as the ASW growth temperature decreases suggests that the Kr atoms can penetrate deeper into the film when it is grown at lower temperatures. Since the Kr atoms travel further on their way to desorption when the films are grown at lower temperatures, the desorption is "delayed". A similar behavior was reported for Xe desorption from solid porous silicon.[28] From growth temperatures of 70 K and higher (including crystalline films), the Kr-atom desorption peak is relatively narrow and occurs at a temperature of 42 K. When 1 ML of Kr is adsorbed on an ASW film grown at 35 K that has been presputtered with 800 eV Ne+ ions for 1 min, the resulting ΔP-TPD profile is identical to that obtained from ASW films grown at temperatures of 70 K or higher. This indicates that while the sputtering of ASW grown at 35 K leads to densification of the top layers of the ASW film, it is likely that the bulk of the film is still porous. Compaction of the entire film to crystallinity is unlikely, given the energy of the Ne+ ions and the eventual removal of water layers as a result of the impact. When ASW

films are grown at temperatures below 60 K, the film contains two types of pores—larger cavities and smaller micropores.[29] When these ASW films are heated, evidence of cavity collapse is observed around 60 K.[6,21] This means that while the Kr atoms can penetrate the ASW cavities, the atoms may be too large to penetrate the ASW micropores. The Ne+ sputtering causes the cavities in the upper layers to collapse into smaller and denser micropores. Since the sputtering experiments are used to determine the distribution of the Kr atoms in terms of location (depth) in the 35 K ASW film, the local (~2 ML deep) structural changes are expected to lead to an error in depth determination of no more than 10−15%, which also reflects the accuracy of our measurements.

located at the bottom (under) the 26 ML thick ASW film, most of the Kr atoms remain in the bottom half of the ASW film. This is seen from the sputtering profiles that show that when 50% of the H_2O molecules are removed from the film, only 37% of the Kr atoms are removed (Figure 1b). When the Kr atoms are initially located in the bottom quarter, the Kr atoms appear to be evenly distributed throughout the ASW (Figure 1c). The sputtering profiles show that when 50% of the H_2O molecules are removed, 52% of the Kr atoms are removed. For these films, no Kr atoms are removed in the first two min of sputtering. Instead, the sputtering apparently causes
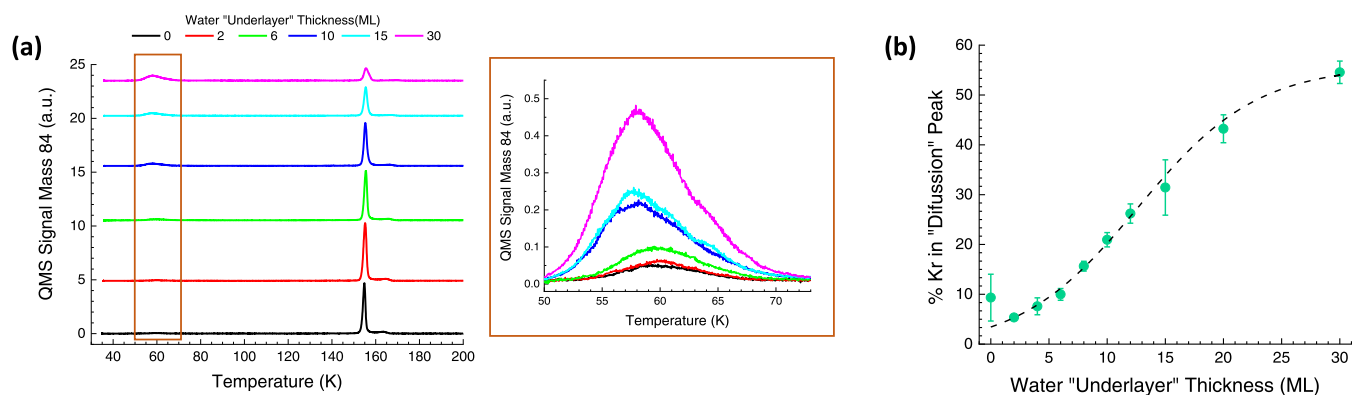
Figure 4. Effect of underlayer thickness of ASW on the amount of Kr located at the ASW−vacuum interface (the diffusion TPD peak). (a) ΔP-TPD measurements of Kr ($m/z = 84$) for 0−30 ML H_2O placed underneath the 2 ML Kr with a fixed overlayer of 13 ML H_2O. The orange box is to bring attention to the low-temperature diffusion peak, which is enlarged to the right of the figure. (b) Percentage of Kr in the diffusion peak as a function of water underlayer thickness (in ML). Sigmoidal fit (dashed line) is to guide the eye. The error bars are derived from the average of two measurements.

the Kr atoms to become more surrounded by the water molecules before removal begins to occur. When Kr atoms are initially positioned in the middle or on top of the film, the Kr atoms are removed at a faster rate than the water molecules (Figure 1d,e). This implies that most of the Kr atoms reside in the top part of the film. Additionally, this suggests that the sputtering does not significantly alter the depth distribution of the Kr atoms throughout the ASW at low temperatures. There appears to be a preference for Kr-atom migration toward the ASW−vacuum interface as opposed to the ASW−substrate interface. This is demonstrated by the removal of 70% of the Kr atoms in the top half of the film (13 ML H_2O) when Kr atoms are initially placed in the middle of the film (Figure 1d). If migration of the Kr atoms within the bulk ASW would occur equally in both directions, the expectation would be for Kr to be evenly distributed throughout the film and then be removed at the same rate as the water molecules. One explanation that can account for the larger amounts of Kr found in the upper half of the ASW film is that the top 13 ML H_2O overlayers displace some Kr atoms and spread them within these top layers.[10] This process occurs in addition to the diffusion of Kr atoms through the ASW pores, which occurs in both directions (toward the Ru−ASW interface and ASW−vacuum interface).

The preference for Kr-atom migration toward the ASW−vacuum interface is further observed when the amount of H_2O adsorbed under 2 ML of Kr ("underlayer") is increased from 0 to 30 ML, while the H_2O overlayer remains set at 13 ML (Figure 4a,b). The Kr ΔP-TPD profiles of these Kr@ASW structures show that as the underlayer amount increases, the low-temperature diffusion peak increases in intensity, while the atomic volcano and trapped peaks both decrease in intensity. This suggests that the underlayer pushes the Kr atoms up toward the ASW−vacuum interface and away from the interior. As the Kr-atom density in the top portion of the film increases, the Kr atoms are more likely to neighbor other Kr atoms. The percentage of Kr atoms near the vacuum interface that desorb in the low-temperature diffusion peak follow a sigmoidal curve as a function of the underlayer thickness. The percentage of Kr atoms that desorb in the low-temperature peak ranges from 5% when the H_2O underlayer is thin to 55% when the H_2O underlayer is thick (Figure 4b). It has been suggested that after the adsorption of 10 ML H_2O on Ru(0001), the subsequent adsorbing layers are no longer in interaction range with the

substrate.[6] This can explain why the Kr atoms are pushed more toward the ASW−vacuum interface as the underlayer nears and surpasses 10 ML H_2O. It is possible that the weakened Kr-atom interaction with the Ru(0001), as a result of the Kr atoms initially being located farther away from the substrate, is what enables them to move more efficiently through the ASW pores toward the ASW−vacuum interface. Additionally, displacement of Kr atoms by incoming water molecules may become more efficient when the water underlayer is thicker.

Although Kr is an inert atom, and obviously does not possess a constant dipole, it is not necessarily totally noninteractive with H_2O. Molecular dynamics simulations show that in solution, Kr atoms prefer to associate with surrounding water molecules rather than form hydrophobic Kr-atom clusters.[30] It is possible that in the cold ASW, the Kr atoms are also surrounded in a solvated-like form by water molecules. As more Kr atoms are brought to the film−vacuum interface, due to displacement by the incoming water molecules, clusters of Kr atoms form. This is seen by an increase in the diffusion peak observed in ΔP-TPD measurements of Kr@ASW films with varying underlayer thicknesses (Figure 4a,b), which indicates an increasing density of Kr atoms near the film−vacuum interface.

3.2. Methyl Chloride (CD_3Cl) Mixing and Distribution in ASW at 35 K. CD_3Cl molecules interact relatively strongly with the Ru(0001) substrate, but relatively weakly with the host water molecules. Nevertheless, compared to the diffusion desorption peak of Kr atoms from the ASW−vacuum interface, the desorption of CD_3Cl molecules in the diffusion peak occurs at a significantly higher temperature. This diffusion peak occurs at the same temperature as the multilayer desorption of CD_3Cl from Ru(0001), and the desorption of CD_3Cl from an ASW film grown at 82 K.[11] As in the case of Kr atoms, the dispersion and mixing of CD_3Cl molecules in ASW is studied through positioning the molecules in different locations within the 26 ML ASW film and monitoring the ΔP-TPD profiles obtained following sputtering by 800 eV Ne^+ ions. The initial position of 2 ML CD_3Cl in 26 ML of H_2O affects the relative intensities of the three observed peaks in the ΔP-TPD spectrum of CD_3Cl ($m/z = 53$) (Figure 5a). As explained in the previous section, the three peaks correspond to the different types of CD_3Cl molecule desorption related to their location and chemical environment within the ASW film. As
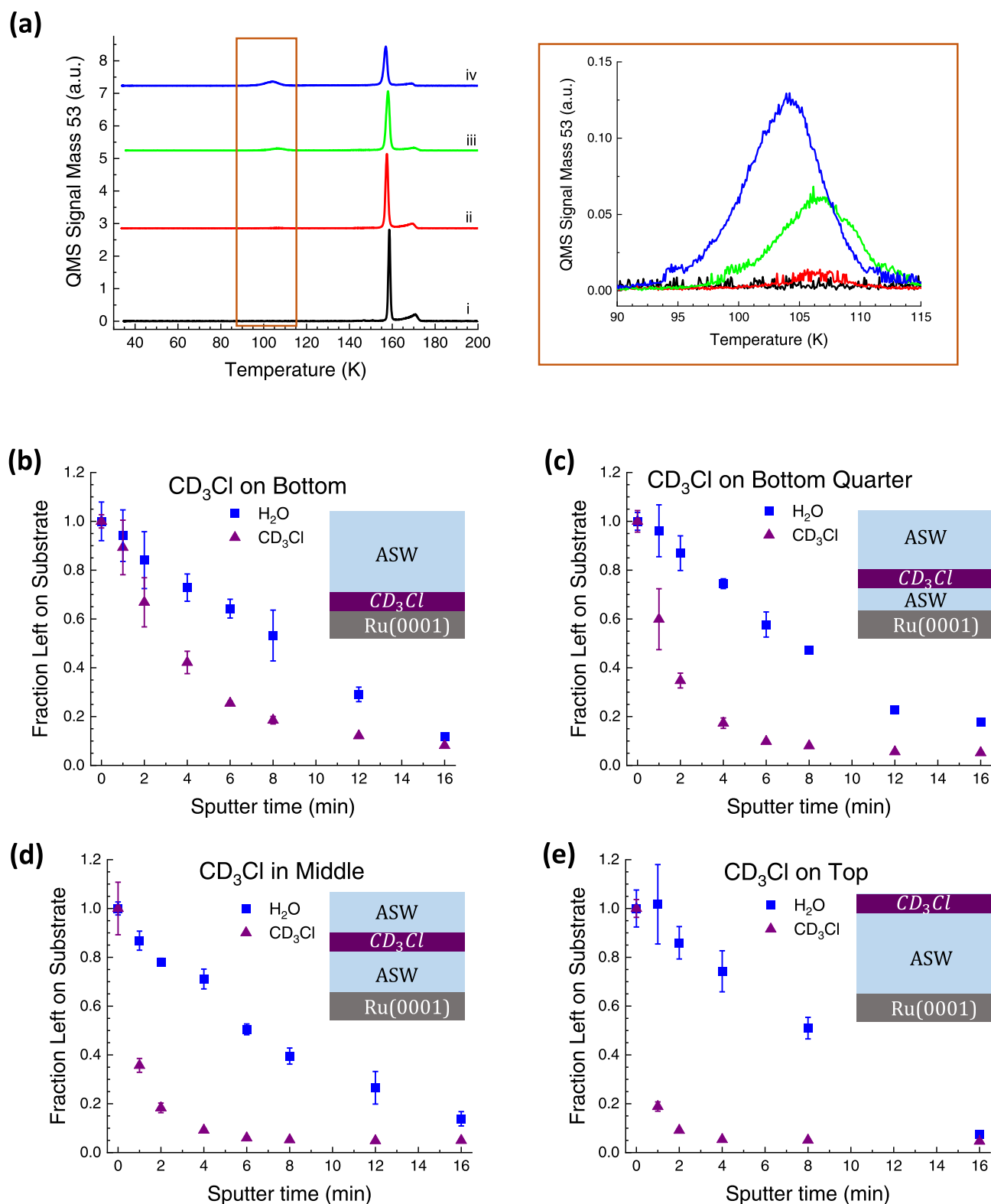
Figure 5. Two ML of CD_3Cl molecules at different initial locations within 26 ML ASW adsorbed at 35 K. (a) Temperature programmed desorption measurements (ΔP-TPD) of CD_3Cl (atomic mass to charge ratio, m/z = 53) at a heating rate of 1 K/s. The orange box is to bring attention to the low-temperature diffusion desorption peak and is enlarged to the right of the figure. (i) 2 ML CD_3Cl initially in direct contact with the ruthenium substrate covered by 26 ML ASW (black), (ii) 2 ML CD_3Cl in the bottom quarter of 26 ML ASW (red), (iii) 2 ML CD_3Cl in the middle of 26 ML ASW (green), and (iv) 2 ML CD_3Cl on top of 26 ML ASW (blue). (b–e) Sputtering of 2 ML CD_3Cl in 26 ML ASW on Ru(0001)@35 K with 800 eV Ne^+ ions ($\sim$2.6 μA) for 0–16 min. The normalized fractions of CD_3Cl (m/z = 53) and H_2O (m/z = 17) remaining on the substrate are plotted versus sputtering time. The error is due to the average of at least two measurements. Plots differ according to the initial position of the 2 ML CD_3Cl in the ASW: (b) bottom (directly on the substrate), (c) bottom quarter, (d) middle, and (e) top.
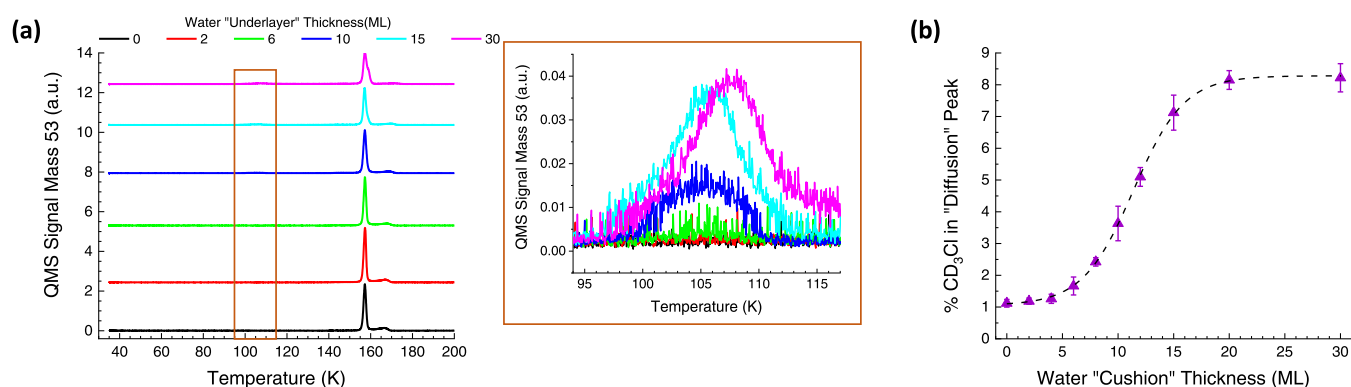
Figure 6. Effect of water layer thickness under CD_3Cl layers on the amount of CD_3Cl molecules found within the ASW surface layers. (a) ΔP-TPD measurements of CD_3Cl ($m/z = 53$) for 0−30 ML H_2O placed underneath the 2 ML CD_3Cl with a fixed overlayer of 13 ML H_2O. The orange box is to draw attention to the low-temperature peak (100−110 K), which is enlarged to the right of the figure. (b) Percentage of CD_3Cl molecules near the ASW surface that desorbs in the low-temperature peak as a function of water underlayer thickness. Sigmoidal fit (dashed line) is to guide the eye. The error bars are derived from the average of at least two measurements.

the initial CD_3Cl position approaches the ASW−vacuum interface, the low-temperature diffusion desorption peak (~103 K) increases in intensity, while the molecular volcano (158 K) and trapped (170 K) peaks decrease in intensity.

Sputtering the $CD_3Cl@ASW$ films with 800 eV Ne^+ ions (~2.6 μA ion current) for 0−16 min at 35 K leads to the slow removal of the film's layers. Subsequently, the ΔP-TPD of each film is recorded to find the distribution of the CD_3Cl molecules throughout the ASW films at 35 K (Figure 5b−e).

For all initial CD_3Cl positions, the CD_3Cl molecules are sputtered at a significantly faster rate than the H_2O molecules. This demonstrates that the majority of the CD_3Cl molecules are located within the upper part of the film, regardless of their original placement. Diffusion of CD_3Cl molecules toward the ASW−Ru(0001) interface was not observed. Figure 5b shows that even when CD_3Cl is placed at the bottom, directly on the Ru(0001) substrate, 83% of the CD_3Cl molecules are removed, while only 50% (13 ML) of the H_2O film is removed following 8 min sputtering. Figure 5c−e shows that as the original CD_3Cl position nears the ASW−vacuum interface, the CD_3Cl molecules are removed almost immediately, in the first few min of sputtering. Similar to the case of Kr atoms, a fraction of the CD_3Cl molecules become surrounded by more water molecules ("solvation"-like) upon sputtering. When CD_3Cl molecules are placed on top of the ASW film, no evidence of increased CD_3Cl molecules' solvation is observed as most of the molecules are removed into the vacuum (80% of the molecules are sputtered within 1 min).

A possible dissociation of the CD_3Cl molecules upon 800 eV Ne^+ ion bombardment was explored but found negligible (seen by tracking D_2 desorption from the Ru(0001) substrate). When the CD_3Cl molecules are initially placed under the ASW film, directly on the Ru(0001) substrate, sputtering of the $CD_3Cl@ASW$ film for 1 min removes only 11% of the CD_3Cl molecules into the vacuum and breaks up clusters of the remaining CD_3Cl molecules. In this way, the number of water neighbors each CD_3Cl molecule interacts with increases. Following 1 min of sputtering, 61% of the molecules desorb in the molecular volcano peak (a decrease from 76% for the nonsputtered film) and 28% of the molecules desorb in the trapped peak (an increase from 24% for the nonsputtered film). No diffusion desorption peak is observed when CD_3Cl is initially placed under the ASW film, since the CD_3Cl molecules that arrive at or are near the ASW−vacuum interface are

mostly surrounded by water molecules and not by other CD_3Cl molecules. As mentioned before, the low-temperature diffusion desorption peak originates from $CD_3Cl−CD_3Cl$ interactions as in its multilayer molecular desorption.

Previous works have shown that when H_2O and CD_3Cl are adsorbed on a Ru(0001) surface either in separate layers or through coadsorption, the H_2O molecules penetrate underneath the CD_3Cl molecules and prevent them from having direct contact with the substrate.[11,12] When H_2O is adsorbed on top of a previously adsorbed CD_3Cl layer, it is likely that the incoming H_2O molecules continue to displace the CD_3Cl molecules until adsorption is complete, causing the CD_3Cl molecules to be spread throughout the ASW overlayers toward the ASW−vacuum interface. Since H_2O molecules attract one another through hydrogen bonding, they prefer to associate with one another, and this displacement process is accelerated when the CD_3Cl molecules are initially sandwiched between H_2O layers. The displaced CD_3Cl molecules can either be isolated in the ASW matrix or compressed into 3D clusters of CD_3Cl molecules of various sizes.[11,31] Small clusters of CD_3Cl can be oriented in such a way that each CD_3Cl is in contact with the surrounding water molecules. In larger clusters, the innermost CD_3Cl molecules will only be surrounded by other CD_3Cl molecules, while the molecules in the outer layer of the CD_3Cl molecular cluster will be in contact with the surrounding water molecules in micelle-like structures.

When a water underlayer is adsorbed underneath the CD_3Cl layer, the amount of CD_3Cl molecules found at the ASW−vacuum interface increases along a sigmoidal curve (Figure 6a,b). A sharp increase in the fraction of CD_3Cl molecules desorbing in the ΔP-TPD diffusion peak occurs between water underlayer thicknesses of 6−15 ML, with an inflection point of 11.3 ML H_2O. This thickness roughly corresponds to the completion of water islands formation on the ruthenium substrate, as discussed in Section 3.1 for the case of Kr@ASW. This suggests that at this H_2O layer thickness, there is no longer any long-range interaction between the ruthenium substrate and the CD_3Cl molecules, and therefore they can more easily be pushed further to the ASW−vacuum interface through displacement. A small shift to a higher temperature of the diffusion desorption peak (Figure 6a) indicates an increase in the number of CD_3Cl molecules interacting with other CD_3Cl molecules at the ASW−vacuum interface. Interestingly, this behavior is the opposite of that observed in the case of Kr
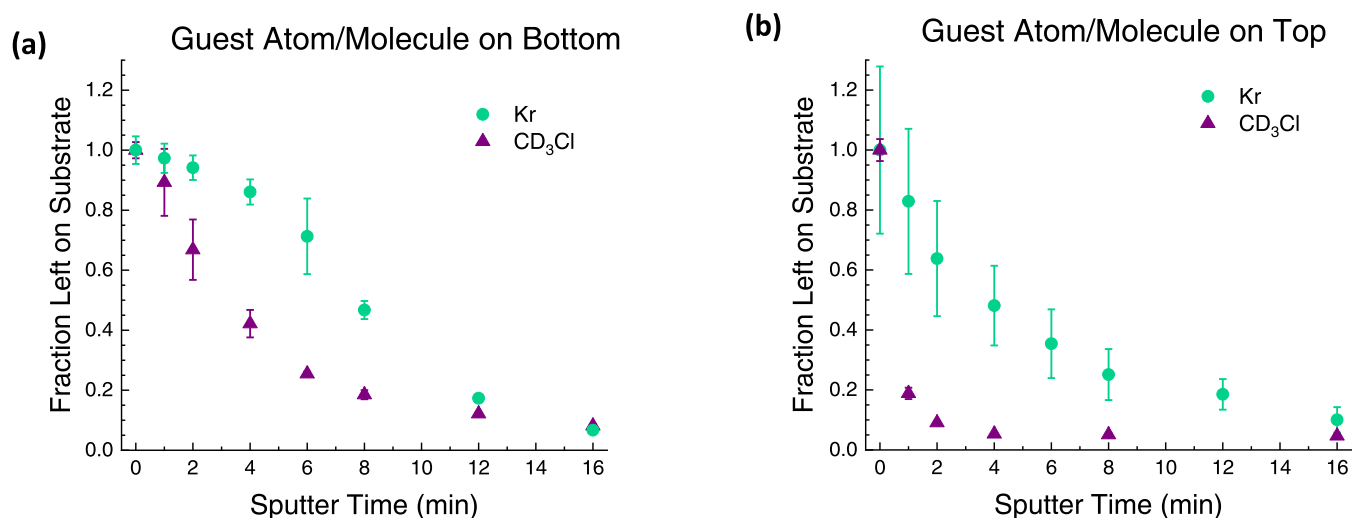
Figure 7. Comparison of the results of sputtering of CD$_3$Cl@ASW and Kr@ASW films at 35 K with 800 eV Ne$^+$ ions (~2.6 μA) for 0−16 min. The normalized fractions of CD$_3$Cl (m/z = 53) and Kr (m/z = 84) remaining on the substrate are plotted versus sputtering time. The error is due to the average of at least two measurements. Plots differ according to the position of CD$_3$Cl/Kr in the ASW (see schemes in Figures 1 and 4): (a) bottom (adsorbed directly on the ruthenium substrate) and (b) on top of the ASW film.

responding to the presence of the water underlayer (see Figure 4a). This is an indication that the CD$_3$Cl molecules are found in clusters at the ASW−vacuum interface and their desorption is similar to a multilayer of CD$_3$Cl (zero order desorption kinetics), while the Kr atoms are more likely to be surrounded by water molecules near and at the ASW−vacuum interface.

For films where 2 ML CD$_3$Cl are placed in the middle of the ASW film, 6% of the CD$_3$Cl molecules desorb in the low-temperature diffusion peak. By contrast, after 1 min of sputtering, 65% of the CD$_3$Cl molecules are removed, while only 14% (~4 ML) of H$_2$O has been removed. Since the desorption peak temperature in ΔP-TPD measurements corresponds to the binding energies of the species to the surface, the ΔP-TPD can qualitatively reveal the chemical surrounding of the species being tracked. These types of measurements cannot strictly give the location of the CD$_3$Cl molecules within the ASW film, but rather give information regarding the molecules' chemical environment. While the majority of the CD$_3$Cl molecules are found in the top layers of the ASW filmthey are not only interacting with other CD$_3$Cl molecules. This suggests that the CD$_3$Cl molecules are compressed and encapsulated into 3D clusters surrounded by water molecules even at the film−vacuum interface. he diffusion desorption peak (100−110 K) is most likely attributed to the desorption of CD$_3$Cl molecules from molecular clusters found in the surface layers of the ASW films. The relatively high desorption temperature of the CD$_3$Cl clusters (compared to that of the Kr desorption peak) is an indication of their stability in the ASW film. Additionally, the desorption temperature is very similar to the multilayer desorption temperature of clean CD$_3$Cl from Ru(0001) that occurs at 100 K, and the desorption of CD$_3$Cl from ASW deposited at 82 K,[11] as mentioned above. The molecular volcano desorption peak at 158 K describes CD$_3$Cl molecules bound to H$_2$O molecules that are only able to desorb upon crystallization of ASW, when the restructuring of the H$_2$O molecules pushes the CD$_3$Cl out of the film.[24,25] Although they desorb upon crystallization of the host water molecules, this does not mean that these CD$_3$Cl molecules are necessarily far (in terms of depth) from the ASW−vacuum interface. The

clustering and encapsulation of the CD$_3$Cl molecules by the surrounding water molecules leads to a higher percentage of CD$_3$Cl molecules desorbing in the molecular volcano peak, even when the CD$_3$Cl molecules are placed on top of the ASW film. Sputtering experiments shown in Figure 5b−e suggest that the relatively strong (compared to Kr−H$_2$O) interaction between CD$_3$Cl and H$_2$O molecules mostly occurs in the upper part of the ASW film.

3.3. Comparison of the Mixing Behavior of Kr@ASW and CD$_3$Cl@ASW at 35 K. Both Kr atoms and CD$_3$Cl molecules preferentially migrate toward the ASW−vacuum interface. A comparison of the post-sputtering ΔP-TPD profiles for Kr@ASW and CD$_3$Cl@ASW where the guest atom or molecule is placed on the bottom of the ASW film, and on top of the ASW film (Figure 7a,b) reveal that compared to Kr atoms, significantly more CD$_3$Cl molecules are found in the upper layers of the ASW film at 35 K. In addition, when Kr atoms are placed on top of the ASW film, they are removed at a slower rate than CD$_3$Cl molecules also placed on top of an ASW film (Figure 7b). This can be explained by understanding the differences in the migration mechanisms for Kr atoms and CD$_3$Cl molecules in ASW. Since Kr atoms can diffuse through ASW pores (when T_{gr} = 35 K), when Kr atoms are placed on top of the ASW film, some Kr atoms will diffuse toward the ASW−Ru interface, further away from the ASW−vacuum interface. This leads to a slower removal rate of Kr atoms compared to CD$_3$Cl molecules placed on top of ASW. Evidence for Kr-atom diffusion is seen in the sputtering profiles for Kr@ASW (Figure 1b−e). In contrast, the CD$_3$Cl molecules cannot penetrate the preadsorbed water film and can only migrate toward the ASW−vacuum interface, primarily through a displacement mechanism by incoming H$_2$O molecules.

The interaction between CD$_3$Cl and H$_2$O in ASW films is dominated by hydrophobic forces. Although the H$_2$O and CD$_3$Cl molecules have a similar (gas phase) dipole moment, the hydrophobicity of CD$_3$Cl molecules (due mostly to the methyl group) dominates the interaction between the two species. Therefore, incoming H$_2$O molecules will replace CD$_3$Cl molecules already bound to preadsorbed H$_2$O

molecules to form more hydrogen bonds. The CD_3Cl molecules are then pushed out of their binding sites and move toward the ASW−vacuum interface, away from the bulk water molecules. As the CD_3Cl molecules are displaced by the surrounding H_2O molecules, they may form stable micelle-like hydrophobic clusters within the ASW, which at higher densities are located near the ASW−vacuum interface. When CD_3Cl molecules are adsorbed on top of ASW films, no mixing occurs except at the top 2−3 ML of the CD_3Cl/H_2O interface. We may conclude that diffusion of CD_3Cl molecules in ASW at 35 K is not observed in these experiments.

As opposed to the CD_3Cl@ASW system, there are no hydrophobic effects at play in the Kr@ASW system. The interaction between Kr atoms and H_2O molecules is weakly attractive. A water molecule generates a relatively large dipolar electric field that is able to polarize a neighbor Kr atom, forming a van der Waals complex.[32,33] Additionally, as explained in Section 3.1, Kr atoms do not form hydrophobic clusters in aqueous environments, but rather each atom becomes individually surrounded by water molecules.[30] Sputtering experiments of Kr@ASW films show that Kr atoms are found in the preadsorbed ASW portion of the film, indicating that Kr atoms can diffuse toward the ASW−Ru interface, penetrating the porous ASW. The mixing of Kr atoms in ASW films is directed by a combination of self-migration and displacement mechanisms. The displacement of Kr atoms by subsequently adsorbed H_2O molecules affects the mixing process, as evidenced by the weak preference for Kr atoms to migrate toward the ASW−vacuum interface.

In the Kr@ASW and CD_3Cl@ASW systems, the interaction (attraction) between neighbor water molecules is stronger than its interaction with Kr atoms or CD_3Cl molecules. Both Kr atoms and CD_3Cl molecules are therefore preferentially pushed to the ASW−vacuum interface since the water molecules prefer to form new hydrogen bonds with each other. Less Kr atoms compared to CD_3Cl molecules are driven to the ASW−vacuum interface because the Kr atoms are less hydrophobic than CD_3Cl molecules and because of their ability to diffuse through ASW pores toward the substrate.

One may question as to what extent the mixing and distribution of the guest atom/molecule in low-temperature ASW we observe is driven by the Ne^+ ion sputtering process. As shown in Figures 2 and 3, the Ne^+ ion sputtering does lead to local structural changes in the ASW film as well as the guest atom/molecule's chemical environment. If the Ne^+ ion sputtering was a main driving force for the observed mixing, we would expect more Kr atoms and CD_3Cl molecules to be found in the lower part of the ASW film (closer to the substrate/ASW interface) since the Ne^+ ions should push the guest atoms/molecules deeper into the film. We have demonstrated that both Kr atoms and CD_3Cl molecules preferentially migrate to the ASW−vacuum interface, indicating that Ne^+ ion sputtering is not a driving force for mixing. Additionally, an atomic volcano peak is observed when Kr atoms are placed on top of ASW, even when the films are subsequently sputtered with 800 eV Ne^+ ions (not shown). Figure 3 shows that this atomic volcano desorption peak is only observed for films grown at temperatures of 45 K and below since they possess larger pores. This is a further evidence that the Ne^+ ion bombardment only leads to a local structural change and does not cause the whole film morphology to be altered. These measurements lead us to the conclusion that the Ne^+ ion sputtering is not a driving force for mixing and

distribution in our systems even if it leads to increased ASW densification at the top 2−3 ML.

4. CONCLUSIONS

The distribution and migration of guest atoms/molecules in thin ASW films deposited at 35 K is dependent on the nature of the guest atom/molecule. Even at this low temperature, there is evidence of atomic/molecular mobility driven by attractive and hydrophobic forces. This enables the guest atoms/molecules to become partially mixed and dispersed within the ASW film. In this study, Kr atoms and CD_3Cl molecules were chosen to represent an atom and a molecule that interact weakly with water. Homogeneous mixing and dispersion within the ASW film was not observed for either Kr atoms or CD_3Cl molecules at this low temperature and for this highly porous ASW film. For both probe species, their initial location in the ASW film affected their distribution within the film, as seen by ΔP-TPD measurements and sputtering−ΔP-TPD experiments. Kr atoms can penetrate ASW pores (when $T_{gr} \leq 45$ K) and can diffuse to some extent either toward the ASW−Ru interface or the ASW−vacuum interface. Additionally, the Kr atoms are spread throughout the upper layers of the ASW film through a displacement mechanism directed by subsequently adsorbed H_2O layers. In contrast, CD_3Cl molecules cannot enter the ASW pores and therefore cannot diffuse through the ASW film at this low temperature. The CD_3Cl molecules migrate to the ASW−vacuum interface primarily via a displacement mechanism that occurs when H_2O molecules are adsorbed on top of preadsorbed CD_3Cl molecules. At the ASW−vacuum interface, the CD_3Cl molecules tend to form aggregates (in the case of 2 ML CD_3Cl, as studied here), as indicated by the diffusion desorption peak, which appears almost exactly at the multilayer desorption temperature of that molecule from the ruthenium substrate, reflecting dominance of CD_3Cl−CD_3Cl intermolecular interactions. Bombardment of the Kr@ASW films by 800 eV Ne^+ induces increased solvation of the Kr atoms near the film−vacuum interface. The initial depth of the Kr atoms does not appear to be significantly altered by ion collisions. For the CD_3Cl@ASW films, bombardment by 800 eV Ne^+ ions preferentially leads to the removal of the CD_3Cl molecules located on top of the ASW film. The difference in the response to sputtering can be (partially) explained by the different masses of Kr (84 amu) and CD_3Cl (53 amu) relative to the collider mass (Ne^+, $m/z = 20$).

More CD_3Cl molecules than Kr atoms are removed in the first layers of the water film following sputtering with Ne^+ ions, indicating that water molecules displace CD_3Cl molecules more effectively than Kr atoms. In the CD_3Cl@ASW system, hydrophobic forces compel CD_3Cl molecules to form micelle-like structures within the ASW, thereby stabilizing the water−CD_3Cl interaction. In contrast, Kr atoms do not form clusters in ASW and prefer to be "solvated" by surrounding water molecules through weak Van der Waals attractive forces. The water molecules' strong attraction to each other and the formation of new energetically favorable hydrogen bonds also dominates the interactions. The abovementioned interactions lead to nonhomogeneous mixing in the ASW matrix at 35 K and can account for the different levels of dispersion for Kr atoms and CD_3Cl molecules. In contrast, when the guest molecule is less interactive toward the host molecule, the mixing will be homogeneous, as in the case of CH_4@ASW mixtures.[34] This was seen in a previous study that employs the

sputtering/ΔP-TPD methods to measure the distribution of CH_4 in mixtures of CH_4@ASW at low temperatures.

■ AUTHOR INFORMATION

Corresponding Author

Micha Asscher − *Institute of Chemistry, The Hebrew University of Jerusalem, Jerusalem 91904, Israel;* ⊙ orcid.org/0000-0002-4476-5617; Email: micha.asscher@mail.huji.ac.il

Authors

Michelle Sykes Akerman − *Institute of Chemistry, The Hebrew University of Jerusalem, Jerusalem 91904, Israel;* ⊙ orcid.org/0000-0001-8652-7513

Roey Sagi − *Institute of Chemistry, The Hebrew University of Jerusalem, Jerusalem 91904, Israel;* ⊙ orcid.org/0000-0001-8872-0683

Hiley Iny − *Institute of Chemistry, The Hebrew University of Jerusalem, Jerusalem 91904, Israel*

Complete contact information is available at:
https://pubs.acs.org/10.1021/acs.jpca.2c06137

Author Contributions

M.S.A. performed all of the experiments, analyzed the data, and wrote the manuscript. R.S. helped in running some of the experiments and developed the LabView code to run the experimental set-up. H.I. helped in conducting some of the experiments. M.A. conceived this study and wrote the manuscript together with M.S.A.

Notes

The authors declare no competing financial interest.

■ REFERENCES

(1) Sandford, S. A. The Inventory of Interstellar Materials Available for the Formation of the Solar System. *Meteorit. Planet. Sci.* 1996, 31, 449−476.

(2) Öberg, K. I. Photochemistry and Astrochemistry: Photochemical Pathways to Interstellar Complex Organic Molecules. *Chem. Rev.* 2016, 116, 9631−9663.

(3) Fayolle, E. C.; Öberg, K. I.; Jørgensen, J. K.; Altwegg, K.; Calcutt, H.; Müller, H. S. P.; Rubin, M.; van der Wiel, M. H. D.; Bjerkeli, P.; Bourke, T. L.; The ROSINA team; et al. Protostellar and Cometary Detections of Organohalogens. *Nat. Astron.* 2017, 1, 703−708.

(4) Acharyya, K.; Herbst, E. Gas-Grain Fluorine and Chlorine Chemistry in the Interstellar Medium. *ApJ* 2017, 850, 105.

(5) May, R. A.; Smith, R. S.; Kay, B. D. The Molecular Volcano Revisited: Determination of Crack Propagation and Distribution During the Crystallization of Nanoscale Amorphous Solid Water Films. *J. Phys. Chem. Lett.* 2012, 3, 327−331.

(6) Sagi, R.; Akerman, M.; Ramakrishnan, S.; Asscher, M. The Role of Thermal History on Spontaneous Polarization and Phase Transitions of Amorphous Solid Water Films Studied by Contact Potential Difference Measurements. *J. Chem. Phys.* 2020, 153, No. 144702.

(7) May, R. A.; Smith, R. S.; Kay, B. D. The Release of Trapped Gases from Amorphous Solid Water Films. I. "Top-down"

Crystallization-Induced Crack Propagation Probed Using the Molecular Volcano. *J. Chem. Phys.* 2013, 138, No. 104501.

(8) Alan May, R.; Scott Smith, R.; Kay, B. D. The Release of Trapped Gases from Amorphous Solid Water Films. II. "Bottom-up" Induced Desorption Pathways. *J. Chem. Phys.* 2013, 138, No. 104502.

(9) Smith, R. S.; Matthiesen, J.; Kay, B. D. Measuring Diffusivity in Supercooled Liquid Nanoscale Films Using Inert Gas Permeation. I. Kinetic Model and Scaling Methods. *J. Chem. Phys.* 2010, 133, No. 174504.

(10) Matthiesen, J.; Smith, R. S.; Kay, B. D. Measuring Diffusivity in Supercooled Liquid Nanoscale Films Using Inert Gas Permeation. II. Diffusion of Ar, Kr, Xe, and CH4 through Methanol. *J. Chem. Phys.* 2010, 133, No. 174505.

(11) Lilach, Y.; Asscher, M. Compression and Caging of CD3Cl by H2O Layers on Ru(001). *J. Chem. Phys.* 2002, 117, 6730−6736.

(12) Maschhoff, B. L.; Iedema, M. J.; Kwini, M.; Cowin, J. P. Long-Range Electrostatic Forces in the Coadsorption of CH3Cl and Water. *Surf. Sci.* 1996, 359, 253−268.

(13) Cyriac, J.; Pradeep, T. Probing Difference in Diffusivity of Chloromethanes through Water Ice in the Temperature Range of 110−150 K. *J. Phys. Chem. C* 2007, 111, 8557−8565.

(14) Bhuin, R. G.; Methikkalam, R. R. J.; Bag, S.; Pradeep, T. Diffusion and Crystallization of Dichloromethane within the Pores of Amorphous Solid Water. *J. Phys. Chem. C* 2016, 120, 13474−13484.

(15) Mayer, E.; Pletzer, R. Astrophysical Implications of Amorphous Ice—a Microporous Solid. *Nature* 1986, 319, 298−301.

(16) Kimmel, G. A.; Stevenson, K. P.; Dohnálek, Z.; Smith, R. S.; Kay, B. D. Control of Amorphous Solid Water Morphology Using Molecular Beams. I. Experimental Results. *J. Chem. Phys.* 2001, 114, 5284−5294.

(17) Westley, M. S.; Baratta, G. A.; Baragiola, R. A. Density and Index of Refraction of Water Ice Films Vapor Deposited at Low Temperatures. *J. Chem. Phys.* 1998, 108, 3321−3326.

(18) Bu, C.; Shi, J.; Raut, U.; Mitchell, E. H.; Baragiola, R. A. Effect of Microstructure on Spontaneous Polarization in Amorphous Solid Water Films. *J. Chem. Phys.* 2015, 142, No. 134702.

(19) Bu, C.; Baragiola, R. A. Proton Transport in Ice at 30−140 K: Effects of Porosity. *J. Chem. Phys.* 2015, 143, No. 074702.

(20) Sagi, R.; Akerman, M.; Ramakrishnan, S.; Asscher, M. Temperature Effect on Transport, Charging, and Binding of Low-Energy Electrons Interacting with Amorphous Solid Water Films. *J. Phys. Chem. C* 2018, 122, 9985−9996.

(21) Akerman, M.; Sagi, R.; Asscher, M. Charging Amorphous Solid Water Films by Ne⁺ Ions Characterized by Contact Potential Difference Measurements. *J. Phys. Chem. C* 2020, 124, 23270−23279.

(22) Ayotte, P.; Smith, R. S.; Stevenson, K. P.; Dohnálek, Z.; Kimmel, G. A.; Kay, B. D. Effect of Porosity on the Adsorption, Desorption, Trapping, and Release of Volatile Gases by Amorphous Solid Water. *J. Geophys. Res.: Planets* 2001, 106, 33387−33392.

(23) Schlichting, H.; Menzel, D. Techniques for Attainment, Control, and Calibration of Cryogenic Temperatures at Small Single-crystal Samples under Ultrahigh Vacuum. *Rev. Sci. Instrum.* 1993, 64, 2013−2022.

(24) Livneh, T.; Romm, L.; Asscher, M. Cage Formation of N₂ under H₂O Overlayer on Ru(001). *Surf. Sci.* 1996, 351, 250−258.

(25) Smith, R. S.; Huang, C.; Wong, E. K. L.; Kay, B. D. The Molecular Volcano: Abrupt CCl₄ Desorption Driven by the Crystallization of Amorphous Solid Water. *Phys. Rev. Lett.* 1997, 79, 909−912.

(26) Dowell, L. G.; Rinfret, A. P. Low-Temperature Forms of Ice as Studied by X-Ray Diffraction. *Nature* 1960, 188, 1144−1148.

(27) Jenniskens, P.; Blake, D. Structural Transitions in Amorphous Water Ice and Astrophysical Implications. *Science* 1994, 265, 753−756.

(28) Paldor, A.; Toker, G.; Lilach, Y.; Asscher, M. Xe Interacting with Porous Silicon. *Phys. Chem. Chem. Phys.* 2010, 12, 6774−6781.

(29) Horimoto, N.; Kato, H. S.; Kawai, M. Stepwise Morphological Change of Porous Amorphous Ice Films Observed through Adsorption of Methane. *J. Chem. Phys.* 2002, 116, 4375−4378.

(30) Watanabe, K.; Andersen, H. C. Molecular Dynamics Study of the Hydrophobic Interaction in an Aqueous Solution of Krypton. *J. Phys. Chem. A* **1986**, *90*, 795−802.

(31) Lilach, Y.; Asscher, M. Photochemistry of Caged Molecules: CD3Cl@Ice. *J. Chem. Phys.* **2003**, *119*, 407−412.

(32) Chal/asiński, G.; Szczęśniak, M. M.; Scheiner, S. Proton−Donor Properties of Water and Ammonia in van Der Waals Complexes with Rare-gas Atoms. Kr−H_2O and Kr−NH_3. *J. Chem. Phys.* **1992**, *97*, 8181−8187.

(33) Aquilanti, V.; Cornicchi, E.; Teixidor, M. M.; Saendig, N.; Pirani, F.; Cappelletti, D. Glory-Scattering Measurement of Water−Noble-Gas Interactions: The Birth of the Hydrogen Bond. *Angew. Chem., Int. Ed.* **2005**, *44*, 2356−2360.

(34) Ramakrishnan, S.; Sagi, R.; Mahapatra, N.; Asscher, M. Effect of Coadsorbed Oxygen on the Photochemistry of Methane Embedded in Amorphous Solid Water. *J. Phys. Chem. C* **2018**, *122*, 15287−15296.

▣ Recommended by ACS